Interfacial compatibility of core-shell cellulose nanocrystals for improving dynamic covalent adaptable networks' fracture resistance (both stress and strain) in nanohybrid vitrimer composites

Journal:	*ACS Applied Materials & Interfaces*
Manuscript ID	am-2023-05041g.R1
Manuscript Type:	Article
Date Submitted by the Author:	n/a
Complete List of Authors:	Sun, Jian; University of Waterloo Liang, Mingrui; University of Waterloo Yin, Lu; University of Waterloo Rivers, Geoffrey; University of Waterloo; University of Nottingham Hu, Guangwei; University of Waterloo; Soochow University Pan, Qinmin; Soochow University, Chemical Engineering Zhao, Boxin; University of Waterloo, Chemical Engineering

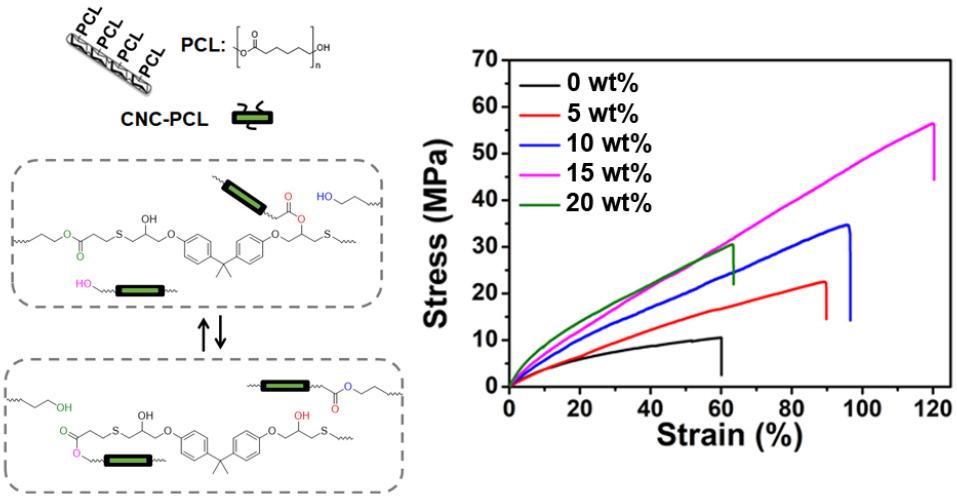

Abstract Graphics

82x44mm (300 x 300 DPI)

Interfacial compatibility of core-shell cellulose nanocrystals for improving dynamic covalent adaptable networks' fracture resistance (both stress and strain) in nanohybrid vitrimer composites

*Jian Sun[1‡], Mingrui Liang[1‡], Lu Yin[1], Geoffrey Rivers[1,2], Guangwei Hu[1,3], Qinmin Pan[3], Boxin Zhao[1]**

[1]Department of Chemical Engineering, Waterloo Institute for Nanotechnology, Centre for Bioengineering and Biotechnology, Institute for Polymer Research, University of Waterloo, Waterloo N2L 3G1, Canada.

[2]Faculty of Engineering, University of Nottingham, Nottingham, NG7 2RD, United Kingdom.

[3]College of Chemistry, Chemical Engineering and Material Science, Soochow University, Suzhou 215123, P. R. China

KEYWORDS: vitrimer, transesterification, cellulose nanocrystals, covalent grafting, poly(ε-caprolactone), elastomeric nanocomposites, fracture resistance

ABSTRACT

The development of polymeric nanocomposites with dynamic covalent adaptable networks and bio-based nanomaterials has been a promising approach towards sustainable advanced materials, enabling reprogramming and recycling capabilities. Herein, a core-shell nanohybrid of functionalized cellulose nanocrystals (CNCs) is explored to provide a crucial interfacial compatibility for improving the covalent adaptable networks of epoxy-thiol vitrimers in fracture resistance. The poly(ε-caprolactone) (PCL) shells grafted from CNC surfaces can be cross-linked with the covalent adaptable networks via a hot-pressing transesterification process. According to the additive concentration and annealing temperature, the stress relaxation behavior of nanohybrid vitrimer composites can be effectively regulated by the core-shell PCL-grafted CNC (CNC-PCL) nanohybrids from dispersed to cross-linked interaction. The addition of 15 wt% of the core-shell

CNC-PCLs exhibits the reinforced improvement of nanohybrid vitrimer composites in average Young's modulus of 2.5 ×, fracture stress of 5.4 × and fracture strain of 2.0 ×. The research findings might have profound implications for developing a synergistic interfacial compatibility between dynamic vitrimer networks and functional nanoparticles for advanced polymeric nanocomposites.

1. INTRODUCTION

Dynamic reconfiguration of covalent adaptable networks (CANs) is crucial for enabling the reprocessing of polymeric materials: exploiting exchangeable chemical bonds allows response to external stimuli, presenting promising applications in repairing, reprograming and recycling.[1-3] Commonly employed exchangeable bond strategies in CANs include dissociative or associative, or mixed.[4] Dissociative networks involve linkages which de-bond, reducing network bond density and network integrity under the applied stimulus, and later reforming and recovering the network when the stimulus is removed. As a result, the material's viscoelastic moduli decrease substantially during the debonding stimulus, such as elevated temperature. In contrast to this, 'vitrimers' are a glass-like type of associative CANs that can simultaneously allow network reconfiguration of exchangeable bond and maintain a constant network integrity in a dynamic

equilibrium system when above a critical topology-freezing transition temperature.[4-6] Such a feature renders vitrimers to be a prospective alternative to classical thermoset polymers, offering minimal creep, while allowing thermal reprocessing without risking structural damage upon heating.[7-9]

Incorporating functional nanofillers into polymer matrixes to formulate the polymeric nanocomposites with tunable properties is a common engineering approach to broaden applicability of polymers, capable of adding functional properties including enhanced mechanical properties and chemical resistance to solvents, or environmental attack by pollution or bacterial.[10-12] Among numerous metal,[13-15] ceramic[16-18] and organic nanoparticles,[19-21] bio-based cellulose nanomaterials have attracted significant interest over the past decade due to their low carbon footprint, abundant raw-source, sustainability, renewability, recyclability, environmental friendliness, biodegradation and non-toxicity.[22,23] Within cellulose-based nanomaterials, cellulose nanocrystals (CNCs) and cellulose nanofibrils (CNFs), display desirable low density (~1.5 g cm^{-3}), axial tensile strength (~5 GPa) and elastic modulus (~150 GPa),[24-26] and they have been employed to produce the reinforced vitrimer nanocomposites by solvent casting, melt processing, layer-by-layer dip coating, spray coating, selective dissolution,

electrospinning and resin impregnation.[12,27,28] To address the processing challenge of nanoscale dispersibility in CANs, extensive efforts have been focused on the bottom-up surface modification of cellulose nanomaterials, including chemical covalent bonding, surfactant treatment, wet compounding, polymer grafting and wrapping.[29-32] Recently, functionalized CNCs have been investigated as cross-linkers to fabricate the nanohybrid CAN composites.[33-35] High concentrations of nanofillers significantly improved the tensile strength of the epoxy nanocomposites cross-linked with carboxylated CNCs (55.5 wt%)[33] as well as the adhesive shear strength of a polydisulfide nanocomposite cross-linked with thiol-functionalized CNCs (30.0 wt%).[34] Yue *et al.* demonstrated a physical ball-milling approach to integrate epoxy thermosets and CNCs for vitrimer nanocomposites,[36,37] achieving 30.0 wt% CNCs displaying an increase in the average Young's modulus from 1.61 GPa to 3.02 GPa[36] and the tensile strength from 62 MPa to 96 MPa.[37] However, CNCs serve as non-mobile obstructions in these nanocomposites, hindering the mobility of the polymer chains near the polymer-nanofiller interfaces and resulting in poor elasticity, reduced fracture strain, and limited fracture stress.[33-37] Thus, it is desirable and challenging to improve the fracture resistance of vitrimer nanocomposites in both stress and strain through the addition of reinforcing fillers such as CNCs.

Herein, we present a core-shell nanohybrid composed of poly(ε-caprolactone) (PCL) polymers grafted-from CNC surfaces, and propose that such functionalized CNCs can provide interfacial compatibility for reinforcement of epoxy-thiol vitrimer composites (Figure 1). We demonstrate not only enhanced the elastic modulus and fracture strength, but also increased the toughness resulting from the elongation of fracture strain. The core-shell PCL-grafted CNCs (CNC-PCLs) were synthesized by the ring-opening polymerization method. The epoxy-thiol polymerization of the vitrimer precursors doped with CNC-PCLs was conducted via an epoxy-thiol 'click' reaction, and then a further cross-linking reaction of CNC-PCLs within the vitrimer matrix was performed via hot-pressing transesterification between the ester and hydroxyl groups of the vitrimer networks and CNC-PCL nanohybrids (Figure 1a). The CNC-PCL nanohybrid vitrimer composites were characterized by thermogravimetric analysis (TGA), differential scanning calorimeter (DSC) measurements and stress relaxation experiments. The carboxylate transesterification exchange reaction of the nanohybrid vitrimer composites (Figure 1b), enabled the cross-linked CNC-PCL nanohybrids to effectively regulate the nanocomposite's stress relaxation behavior. Furthermore, the cross-linking interaction between the CNC-PCLs and vitrimer networks provided the network reinforcement, improving the mechanical performances

of nanohybrid vitrimer composites in terms of Young's modulus (2.5 ×), fracture strain (2.0 ×), and fracture stress (5.4 ×). This work introduces a novel strategy to fabricate functional nanocomposites with enhanced interaction between a polymer matrix and nanomaterials, enabling future bio-derived re-processible engineering composites.

2. EXPERIMENTAL SECTION

2.1. Materials. ε-caprolactone, polycaprolactone diol (PCLOH, Mn = 2000 g mol^{-1}), 3-mercaptopropionic acid, pentaerythritol tetrakis(3-mercaptopropionate) (PETMP), bisphenol A diglycidyl ether (BADGE), triazabicyclodecene (TBD), 3-mercaptopropionic acid, 1,8-diazabicyclo[5.4.0]undec-7-ene (DBU), tin(II)ethylhexanote ($Sn(Oct)_2$), citric acid, hydrochloric acid (HCl, 37%), thionyl chloride ($SOCl_2$), potassium iodide (KI), potassium carbonate (K_2CO_3), magnesium sulfate ($MgSO_4$), sodium bicarbonate ($NaHCO_3$), N,N-dimethylformamide (DMF) acetone, toluene, hexane, dichloromethane (DCM), ethyl acetate (EtOAc) and acetonitrile were purchased from Sigma-Aldrich. CNC (NCV100 - NASD90) was supplied by CelluForce Inc. (Canada).

2.2. Experimental Methods. *Nuclear Magnetic Resonance Spectroscopy*. ^{1}H spectra were recorded on a Bruker 300 MHz spectrometer. Chemical shifts (δ) are denoted in parts per million (ppm) relative to the residual solvent peak ($CDCl_3$, $\delta = 7.26$).

Fourier Transform Infrared Spectroscopy. Attenuated total reflection Fourier transform infrared (ATR-FTIR) measurements were recorded on a Bruker TENSOR 27 spectrometer in a spectral range of 4000-400 cm^{-1}.

Transmission Electron Microscopy. CNC suspensions (0.1 g/L in DI water) and CNC-PCL suspensions (0.1 g/L in acetone) were prepared by sonication for 10 min. Transmission electron microscopy (TEM) images were taken by a Jeol 1200EX.

Dynamic Light Scattering Measurement. CNC suspensions (1.0 g/L in DI water) and CNC-PCL suspensions (1.0 g/L in acetone) were prepared by sonication for 15 min at 25 °C. Dynamic light scattering (DLS) analysis was taken by a Malvern Zetasizer Nano ZS90 working at a 90° scattering angle.

Atomic Force Microscopy. CNC suspensions (0.01 g/L in DI water) and CNC-PCL suspensions (0.01 g/L in acetone) were deposited on a cleaved mica plate. After air-drying, the samples were imaged by an atomic force microscope (AFM) Dimension 3100 (Veeco Metrology Group) with tapping mode.

Water Contact Angle Measurements. Sessile drop technique was used by a custom-made apparatus. Droplets of DI water (3.0 μL) was dispensed with a microsized needle through a syringe pump (New Era Pump System Inc.). CNC suspensions (1.0 g/L in DI water) and CNC-

PCL suspensions (1.0 g/L in toluene) were coated on glass substrate, respectively, and then were dried in an oven at 80 °C overnight. Vitrimer films were prepared by hot-pressing on glass substrate at 160 °C and 5 MPa for 24 h. At least five images of the liquid droplets deposited on the sample surfaces were analyzed.

X-Ray Photoelectron Spectroscopy. CNC and CNC-PCL samples were prepared by coating the suspensions on a glass substrate as described above. High resolution X-Ray photoelectron spectra (XPS) were recorded on a VGS ESCALab 250 system.

Swelling Ratio and Gel Fraction Measurements. The vitrimer samples with the dimension of 5 mm × 5 mm ×1 mm were swollen in toluene for 24 h at 80 °C. After swelling, the samples were wiped and weighed. The swelling ratio was calculated by $(W_S-W_I)/W_I \times 100\%$, where W_I and W_S are the weights before and after swelling, respectively. Then the samples were dried in a vacuum oven for 24 h at 80 °C, and the dried weight W_D is used to calculate the gel fraction by $W_D/W_I \times 100\%$.

Thermogravimetric Analysis. The thermal stability was characterized by TGA using a TA Instruments Q500. The samples were analyzed from room temperature to 600 °C with a heating rate of 10 °C min^{-1} under nitrogen flow.

Differential Scanning Calorimetry. DSC measurements were performed by a TA Instruments Q2000 under the nitrogen flow. A pre-scanning test was conducted by heating up to 150 °C, and holding for 10 min to eliminate the thermal history. Then the scanning cycles was recorded between -90 to 150 °C at a rate of 10 °C min^{-1}.

Dynamic Mechanical Analysis. Stress relaxation experiments were conducted with vitrimer samples measuring 20 mm × 5 mm × 1 mm using a TA Instruments Q800 in tensile mode, at four selected test temperatures (150, 160, 170, 180 °C). After temperature equilibration for 5 min, a constant 10% strain was applied, and the stress was recorded over time.

Stress-Strain Tensile Measurements. The vitrimer samples with the dimension of 20 mm × 5 mm × 1 mm were tested by a Universal Material Tester (UMT, Bruker, USA) at a strain rate of 100 μm s^{-1}. The strain to failure, tensile stress at failure and Young's modulus were calculated from the tensile measurements of at least 5 replicates.

Scanning Electron Microscopy. The vitrimer samples were cut off previously. The fractured surfaces were gold-coated and observed by scanning electron microscopy (SEM, Zeiss FESEM 1530).

2.3. Preparation of CNC-PCL. Solvent-exchange of the CNC suspension (50 g/L in DI water) was performed through wet transfer with acetone, and then with anhydrous toluene by several successive centrifugation and redispersion operations (at least 3 cycles). A sample of this dispersion of CNC (1.0 g) in toluene (100 mL) was stirred under nitrogen atmosphere for 30 min at 110 °C. After then, a mixture of ε-caprolactone (5.0 g), $Sn(Oct)_2$ (0.2 mL) and citric acid (0.2 g) in toluene (20 mL) was dropwise added. The ring-opening polymerization was allowed to proceed for 24 h and was stopped by adding a few drops of HCl solution (1 M). The obtained product was centrifuged after the precipitation by adding hexane. To remove the free PCL chains, the resulted CNC-PCL was purified by Soxhlet extraction with DCM for 24 h, after which it was allowed to redispersed in toluene.

2.4. Synthesis of PCLSH. The synthetic process of PCLSH is shown in Figure S1. To a solution of PCLOH (20.0 g, 10.0 mmol) in DCM (100 mL), $SOCl_2$ (2.97 g, 25.0 mmol) was added. The mixture was stirred for 24 h at 60 °C. After the mixture was cooled down, DI water (50 mL) was carefully added and the mixture was extracted with DCM (3 x 50 mL). The organic layers were washed with $NaHCO_3$ (saturated aqueous solution, 50 mL) and HCl (1M), and dried on $MgSO_4$. The solvent was removed in vacuum and the residue was dried in a vacuum oven for 24 h at 80 °C to yield PCLCl as a lightly yellow solid (17.4 g, 85.4%). ^{1}HNMR (300 MHz, $CDCl_3$) at this stage reported the following: δ = 4.05 (t, J = 6.6 Hz, 32H), 3.87 (s, 4H), 3.52 (t, J = 6.6 Hz, 4H), 2.31 (dd, J = 14.8, 7.3 Hz, 36H), 1.62 (dd, J = 14.1, 6.9 Hz, 68H), 1.44 - 1.28 (m, 32H) (Figure S2). To a solution of PCLCl (10.0 g, 4.9 mmol) in DMF (100 mL), a mixture of 3-mercaptopropionic acid (1.168 g, 11.0 mmol), DBU (0.336 g, 2.2 mmol), KI (0.360 g, 2.2 mmol) and K_2CO_3 (1.658 g, 12.0 mmol) was added. The mixture was stirred for 24 h at 95 °C. After the mixture was cooled down, DI water (50 mL) was added slowly, and the mixture was then extracted with EtOAc (3 x 50 mL). The organic layers were washed with HCl (1M) and $NaHCO_3$ (saturated aqueous solution, 50 mL), and dried on $MgSO_4$. The solvent was removed *in vacuo* and the residue was dried in a vacuum oven for 24 h at 100 °C to yield PCLSH as a lightly yellow solid (8.7 g, 81.6%). ^{1}HNMR (300 MHz, $CDCl_3$) at this stage reported: δ = 4.07 (t, J = 6.6 Hz, 32H), 3.89 (s, 4H), 2.88 - 2.47 (m, 8H), 2.33 (dd, J = 15.4, 7.9 Hz, 36H), 1.75 - 1.55 (m, 72H), 1.39 (dt, J = 9.4, 7.6 Hz, 34H) (Figure S3).

2.5. Preparation of epoxy-thiol vitrimer. To a mixture of BADGE (250 mg, 0.734 mmol, 100 mol% of epoxy functional groups), PCLSH (958.7 mg, 0.440 mmol, 60 mol% of thiol functional groups) and PETMP (71.8 mg, 0.147 mmol, 40 mol% of thiol functional groups) in

anhydrous toluene (0.5 mL), a desired amount of the CNC-PCL in toluene from Section 2.3 was added according to the corresponding mass fraction of CNC-PCL (0, 5, 10, 15 and 20 wt%), followed by sonication for 15 min. Afterwards, the catalyst TBD solution (0.15 mL, 10% w/v in acetonitrile, 1.2 wt%) was added and the mixture was sonicated in a bath for 20 min before casting into a polytetrafluoroethylene mold. The samples were heated at 100 °C for 2 h to remove the residual toluene, and then heated up to and maintained at 140 °C for 24 h to conduct the epoxy-thiol polymerization of vitrimer precursors. The obtained vitrimers are denoted as V*x*, where *x* is the mass fraction of the CNC-PCL ($x = 0$, 5, 10, 15 or 20). The cross-linking reaction of the CNC-PCLs in the epoxy-thiol vitrimers was performed via the transesterification exchange reaction under hot-pressing at 160 °C and 1 MPa for 8-48 h.

3. RESULTS AND DISCUSSION

3.1. Chemical Modification of CNCs. "Grafting from" of PCL polymers to the surfaces of CNCs is a well-established approach to improve their hydrophobic compatibility in guest-host nanocomposites.[38,39] To further enhance the PCL grafting efficiency for cross-linking to vitrimer systems, the *in-situ* catalyzed ring-opening polymerization method was used to graft PCL polymers from CNC surfaces via organic acid-catalyzed improvement (Figure 2a), where citric

acid provides acid moieties and α-hydroxy groups to assist the ring-opening polymerization of lactones.[40] From TEM characterization, the micromorphology of the core CNC exhibited rod shapes (Figure S4). After organic acid-catalyzed ring-opening polymerization, the surface-grafted PCL polymer chains obviously increased the length and the diameter of CNC-PCL (Figure 2b). To better confirm the morphology evolution from CNC to CNC-PCL by DLS and AFM, the rod length was characterized by the Z-average size from 132.4 nm (PDI = 0.313) to 398.3 nm (PDI = 0.264), where PDI is polymer dispersity index (Figure 2c), and the rod diameter was determined by the height of topological profiles from 6 ± 1 nm to 12 ± 3 nm (Figure 2d).

To investigate the structural effect of the chemical modification, the CNCs before and after PCL grafting were characterized by FTIR spectroscopy, water contact angle and high-resolution XPS spectrometry. After Soxhlet extraction, the presence of grafted PCL polymers can be confirmed by the intense peak of carbonyl group of carboxylic ester (C=O, 1726 cm^{-1}) of the CNC-PCLs compared to the FTIR spectrum of CNCs (Figure 3a). In the water contact angle experiments, the water droplets partially spread on the surface of CNC coating, demonstrating the hydrophilic performance with a contact angle of 24.0 ± 2.0° (Figure 3b, top). However, in the case of CNC-PCL coating, the hydrophobic performance of PCL chains was observed with a

contact angle of 86.7 ± 1.0° (Figure 3b, bottom). The XPS spectra show that the carbon and oxygen atoms are the main elements of the CNC and CNC-PCL (Figure S5). The PCL grafting efficiency can be analyzed by the high-resolution C1s peak resolved into various carbon components (A: C-C/C-H_x, 284.8 eV; B: C-OH, 286.3 eV; C: O-C-O, 287.4 eV; D: O-C=O, 288.8 eV) (Figure 3c). The relative amounts of each were calculated by the corresponding integral areas as listed in Table 1. Notably, the increased C1s D signal indicates that the relative amount of carboxylic ester groups in the grafted PCL chains reached 18.06% in the CNC-PCLs, while the low relative amount in the pure CNCs (3.83%) might be attributed to the residual cell wall polysaccharides with the carboxylic groups.[38] The above results suggest the PCL polymers have been covalently grafted onto the surface of CNCs, leading to the core-shell nanostructure of the CNC-PCL nanohybrids with hydrophobic performance.

3.2. Formation of Vitrimer Networks Cross-Linked with CNC-PCLs. After introducing the CNC-PCLs into the vitrimer precursors and performing the epoxy-thiol 'click' vitrimer polymerization, the CNC-PCL nanohybrids are dispersed in the vitrimer networks without obvious aggregation. Thereafter, both the vitrimer networks and the dispersed CNC-PCLs intrinsically have the hydroxyl groups and the ester bonds, available for the carboxylate transesterification exchange reaction between the CNC-PCLs and the vitrimer networks during hot-pressing (Figure 1a). The cross-linking behavior of nanohybrid vitrimer networks was analyzed using the swelling ratio and gel fraction. As shown in Figure 4a, the virgin vitrimer V0

displays an average swelling ratio of 146.0%, and the swelling ratios of the vitrimers doped with different CNC-PCL contents (V5, V10, V15 and V20) had a slight reduction but were still above 100.0% before the hot-pressing transesterification. After cross-linking reaction for 24 h, the swelling ratio of V0 slightly decreased to 134.0 ± 6.3%, while the vitrimers cross-linked with CNC-PCLs exhibited the reduction in the swelling ratio from 92.0 ± 3.2% to 29.0 ± 2.8% with increasing the content of the CNC-PCLs from 5 to 20 wt%. It indicates that the bonded-to CNC-PCLs act as the extra cross-linking points to enhance the cross-linking density of vitrimer networks after transesterification exchange reaction. Furthermore, the gel fractions of the vitrimers remained constant around 80% before and after the cross-linking reaction (Figure 4b). It suggests that the dynamic exchangeable bonding behavior of the CNC-PCLs occurs in the rearranged network of the epoxy-thiol vitrimers with fixed cross-linking points. Due to the hydrophobic property of CNC-PCLs, there is little influence on the contact angle of the nanohybrid vitrimer composites when it is above 80.0° (Figure 4c).

3.3. Thermal Properties of Nanohybrid Vitrimer Composites. The thermal behaviors of the vitrimer cross-linked with CNC-PCLs were investigated by the DSC cycle measurement for the melting point (T_m), melting enthalpy (ΔH_m) and glass transition temperature (T_g) in heating curves, and the crystallization temperature (T_c) and crystallization enthalpy (ΔH_c) in cooling

curves (Figure 5a). As summarized in Table 2, the CNC-PCL nanohybrids exhibited T_c = 31.95 °C and T_m = 53.20 °C, which are attributed to the crystalline structure of PCL chains. Compared to the typical T_m of the PCL around 60 °C, the lower T_m of the CNC-PCL nanohybrids is probably because of the low polymerization degree of the grafted PCL polymers.[38,41] The melting transition and crystallization of virgin vitrimer V0 is contributed by the PCLSH components. With the increase in the content of the cross-linked CNC-PCLs, the T_c, T_m, ΔH_c and ΔH_m of the nanohybrid vitrimer composites firstly decreased with 5 wt% CNC-PCLs, and then gradually increased with 15-20 wt% CNC-PCLs, indicating the increased degree of crystallinity of the corresponding nanohybrid vitrimer composites with a larger amount of PCL units. Furthermore, the single endothermic/exothermic peaks suggest the excellent nanofiller-matrix compatibility between the CNC-PCLs and the epoxy-thiol polymers. In addition, the T_g of the vitrimer composites V0-V20 increasing from -42.31 to -11.96 °C is mainly resulted from their correspondingly enhanced cross-linking density with increasing the content of CNC-PCL nanohybrids from 0 to 20 wt% (Table 2 and Figure S6).

The thermal stability of the CNC-PCL nanohybrids and the vitrimer composites was analyzed by the TGA curves (Figure 5b). For the CNC-PCL nanohybrids, a first mass loss of 8 wt% occurred at 25-250 °C probably owing to the water and volatile products, and a second mass loss of 19 wt% appeared with an onset degradation temperature (T_{onset}) of 255 °C and a maximum degradation temperature (T_{dmax}) of 267 °C attributed to the partial short PCL chains in the grafted PCL shell of the CNC-PCL nanohybrids.[42,43] In contrast to the CNCs, the T_{onset} and T_{dmax} of the CNC-PCL nanohybrids increased from 305 to 380 °C and from 320 to 408 °C, respectively

(Figure S7). It suggests that the grafted PCL shell can enhance the thermal stability of CNC-PCL nanohybrids due to the higher thermal stability of PCL polymers.[42,44] Based on the residue of pure CNCs at 600 °C, approximately 19 wt%, the CNC content of CNC-PCL nanohybrids was calculated by dividing the residue of CNC-PCL nanohybrids (~5 wt%, 600 °C) by the residue of pure CNCs (~19 wt%, 600 °C) to be 5/0.19 = ~26 wt%, suggesting the effective grafting of the PCL shell at around 74 wt%. For all the vitrimer composites, the similar T_{onse} and T_{dmax} were found at around 375 °C and 415 °C, respectively. Compared to the residue of virgin vitrimer V0 around 1 wt% at 600 °C, the other vitrimers cross-linked with CNC-PCLs exhibited an increased residue of around 5 wt% from the residual CNCs. It demonstrates the incorporation of CNC-PCLs has minimal effect on the thermal stability of vitrimers.

3.4. Dynamic Mechanical Properties of Nanohybrid Vitrimer Composites. For typical vitrimer materials, the dynamic bond exchange of CANs was commonly analyzed by stress relaxation experiments at several temperatures.[4] As shown in Figure 6a-e, the stress of all vitrimer composites can be relaxed to 1/*e* (36.8%) of the initial stress (σ_0) at 150-180 °C, and the stress relaxation sped up with the increase in temperature. Based on the Maxwell model and the generalized Maxwell model, the normalized stretched stress (σ/σ_0) over time (t) is well fitted by a second-order exponential decay equation:

$$\frac{\sigma}{\sigma_0} = \frac{\sigma_1}{\sigma_0} e^{-t/\tau_1} + \frac{\sigma_2}{\sigma_0} e^{-t/\tau_2} + A_0 \quad (1)$$

where σ is the stress, τ is the relaxation time and A_0 is the minimum σ/σ_0 at infinite time. As listed in Table S1, the fitting results of stress relaxation contain a rapid Stage 1 ($\tau_1 < 12$ min) and a long-term Stage 2 ($\tau_2 > 98$ min) with all adjusted $R^2 > 0.990$, where R is the correlation coefficient. Such two-stage stress relaxation indicates a widespread distribution of the strength of polymer chain confinement in the vitrimer systems.[45] The short stress relaxation (Stage 1) is mostly associated to the normal relaxation of the cross-linked polymer in response to the mechanical stimuli, resulting from energy dissipation by internal frictional resistance of intermolecular mechanical motion, and the molecular chain conformation change.[46-48] The long-term stress relaxation (Stage 2) is mostly attributed to the transesterification reaction between ester and hydroxyl groups: for exchange of reconfigurable ester bonds at high temperature. Due to the larger time scale of τ_2, the whole stress relaxation is dominated by the transesterification reaction sensitive to temperature. After the incorporation of cross-linked CNC-PCLs in vitrimer networks, there are two competing factors that can impact the stress relaxation behaviors. Factor 1 is the additional concentration of ester and hydroxyl moieties from the grafted PCL shell of CNC-PCLs, which can positively promote the transesterification exchange rate of the vitrimer systems.[36,49,50] Factor 2 is the CNC-PCL nanohybrids serving as non-mobile obstructions that can negatively impede the thermomechanical motion of surrounding polymer chains to slow

down the stress relaxation of the vitrimer networks, similar to the anchoring effect of silica nanoparticles in CAN nanocomposites.[51-53] The competition between these two factors at different annealing temperatures causes the nanohybrid vitrimer composites to exhibit the a lower τ_2 (faster relaxation) due to the dominant influence of Factor 1 at a low temperature, such as the decrease from 247.9 min for V0 to 184.9 min for V20 at 150 °C (Table S1), while the slower stress relaxation is caused by the dominance of Factor 2 at high temperature, such as the increase of the relaxation time from 117.8 min for V0 to 152.3 min for V20 at 180 °C (Table S1).

Transesterification is a dynamic temperature-dependent equilibrium process, and so the stress relaxation behavior of the vitrimers can be described using the Arrhenius law:[5,7]

$$ln(\tau_2) = \frac{E_a}{RT} + ln(\tau_0) \quad (2)$$

where E_a is the activation energy of transesterification reaction, R is the gas constant, T is the absolute temperature and τ_0 is the Arrhenius pre-factor time constant. The linear fitting curves of the $\ln(\tau_2)$ versus $1000/T$ are shown in Figure 6f, and the fitting parameters are listed in Table 3. For vitrimers in practical applications, the E_a value describes not only the barrier for intentional activation of stress relaxation in response to the topology freezing transition temperature, but also the sensitivity of unintentional stress relaxation behavior in response to the variation in temperature.[54] By increasing the CNC-PCL nanohybrids content, the vitrimer composites exhibited the E_a values reduced from 38.67 kJ/mol for V0 to 10.20 kJ/mol for V20, indicating the

characteristic stress relaxation of V20 can possibly reach 1/*e* of the initial stress at lower temperature caused by Factor 1. On the other hand, the decrease in the E_a and the increase in the $\ln(\tau_0)$ reduce the variation of characteristic relaxation time ($\Delta\tau_2$) from 130.1 min for V0 to 32.6 min for V20 (between 150 and 180 °C), respectively. This is attributed to the less pronounced viscosity change of the vitrimer networks with increased CNC-PCLs caused by Factor 2. It suggests the relatively slow stress relaxation of V20 (152.3 min) compared to that of V0 (117.8 min) at higher temperature (180 °C). The above results demonstrate the cross-linked CNC-PCLs can effectively regulate the stress relaxation behavior of nanohybrid vitrimer composites.

3.5. Reinforcing Mechanical Properties of Nanohybrid Vitrimer Composites. Mechanical properties of the nanohybrid vitrimer composites were measured by strain under uniaxial tension. The epoxy-thiol vitrimers doped with CNC-PCL nanohybrids but without hot-pressing transesterification exhibited an obvious elastic-plastic transition in the strain-stress curves (Figure 7a). For increasing CNC-PCL contents, both Young's modulus (E_t) and stress at failure (ε_f) increased from E_t = 48.5 ± 8.4 MPa and ε_f = 10.4 ± 0.6 MPa for V0 to E_t = 300.2 ± 47.3 MPa and ε_f = 43.9 ± 2.1 MPa for V20 (details are shown in Table S2). Interestingly, the strain to failure (σ_f) firstly increased from 59.9 ± 4.0% for V0 to 79.1 ± 5.8% for V10, but then decreased to 67.7 ± 6.6% for V15 and 54.2 ± 7.7% for V20. As shown in the SEM images of fractured surfaces, there is no obvious aggregation in V0, V5 and V10 (Figure S8a-c). However, the micron-sized aggregates of 0.41 ± 0.05 μm and 1.11 ± 0.68 μm were found in V15 and V20, respectively (Figure S8d-e). It suggests that the uniformly dispersed CNC cores (≤ 10 wt%)

enhance the tensile movement of polymer chains, while the larger amount of CNC-PCL nanohybrids (≥ 15 wt%) would agglomerate into the micron-sized particles and afterwards suppressed the mobility of polymer chains, which is in agreement with the previous reports.[38,44]

To investigate the transesterification effect on the mechanical properties of the vitrimer composites over time, the strain-stress curves of varying compositions were characterized after hot-pressing upon 1 MPa for varying times at 160 °C. The virgin vitrimer V0 did not show any obvious change over 48 hours (Figure S9a). In comparison, the plastic region of strain-stress curves of the nanohybrid vitrimer composites became unclear with a decrease in E_t at first, followed by their mechanical properties generally stabilized in 16 hours (Figure S9b-e), indicating that the cross-linking of the CNC-PCL nanohybrids with their vitrimer matrix networks reached equilibrium after 16 hours. Notably, the mechanical performances of the nanohybrid vitrimer composites reinforced with the increasing cross-linked CNC-PCLs from 0 to 15 wt%, and V15 exhibited the greatest improvement of ε_f = 56.5 ± 1.8 MPa and σ_f = 119.8 ± 8.8% (Table S2). Compared with the dispersed interaction with the vitrimer networks, the cross-linked CNC-PCL nanohybrids of 15 wt% can significantly improve the elasticity of the nanohybrid vitrimer composites for the fracture resistance in stress of 1.4 × and strain of 1.8 × (Figure 7b). Due to the core-shell nanostructures (Figure 2), the PCL shells act as the buffered interfaces both covalently wrapping the CNC cores and cross-linking to the vitrimer networks. The enhanced elasticity suggests such interfacial compatibility can reduce the impeding effect of

CNC-PCL nanohybrids on the stretched mobility of polymer chains. To compare with the CNC/CNF-vitrimer systems in literatures, the relative reinforcing ratios in stress and strain are listed in Table S3, where percentage of stress reinforcement (%) and percentage of strain reinforcement (%) are calculate by (reinforced - initial)/initial × 100%, respectively. It indicates this work is more effective than the other vitrimer nanocomposites containing with CNCs[35-37,55] and CNFs.[56,57] However, the over-aggregations of the CNC-PCL nanohybrids (20 wt%) still displayed a remarkable impeding effect caused by Factor 2 as explained in Section 3.4, leading to the poor elasticity and reduced ε_f for V20 during the cross-linking process (Figure S9e).

Finally, we performed mechanical tests to demonstrate the nanohybrid vitrimer composite V15 capable of recycling, reprograming and shape memory recovering. As shown in Figure 8a, the nanohybrid vitrimer composite was cut into small pieces, and then the integrated bulk was reprogramed via hot-pressing recycling with the cracked pieces upon 1 MPa at 160 °C for 16 hours. Although the yellow colour of the vitrimer composites, including the virgin vitrimers, darkened upon thermal treatment over time, the darkening processes were similar and their mechanical properties displayed no obvious degradation after third recycling process (Figure 8b). To further check the reason of darkening process, all vitrimer composites were thermally treated in nitrogen atmosphere at 160 °C for 16 hours. It was found the extent of darkening were greatly weaker than the thermal treatment under air atmosphere (Figure S10). These suggest that the

darkening process was mainly related to the oxidation reaction of vitrimer network. Here the recycling and reprograming process is mainly dependent on the rate of the carboxylate transesterification reaction. Further research is needed to explore the modification of the hydroxy end group of PCL shells, and to apply these nanohybrid strategies for various exchange kinetics based on specific exchangeable bonds of vitrimers, including siloxane exchange, olefin metathesis, disulfide metathesis, imine-amine exchange, and boronic-based exchange.[58-60] Despite the *Tg* of vitrimer composites being lower than 0 °C, their temporary shapes can be programmed via mechanical deformation as a result of the crystalline structure of PCL chains at room temperature[61-63] For example, a length of vitrimer composite was stretched from 10 cm to 15 mm, as highlighted by the black line in Figure 8c. The programmed nanohybrid vitrimer composite can then be recovered to the initial shape via heating above T_m, resulting from the triggered elasticity of PCL chains responsible for the thermal phase transition. In this work, the PCL components are employed in both the epoxy-thiol vitrimer networks and the CNC-PCL nanohybrids to enable the elastic shape memory. Further increase in the amount of PCL chains in CNC-PCL nanohybrids has a great potential to endow the PCL-free polymeric nanocomposites with the capability of shape memory for applications in soft actuators and soft robots.

4. CONCLUSIONS

In summary, a novel integrated nanocomposite was demonstrated, composed of a vitrimer matrix of epoxy-thiol CANs, cross-linked to core-shell CNC-PCL nanohybrids via epoxy-thiol 'click' reaction and hot-pressing transesterification process. The resultant nanohybrid vitrimer composites revealed that the cross-linked CNC-PCL nanohybrids can not only effectively regulate the stress relaxation behavior of the vitrimers and the activation energy of the transesterification reaction, but also significantly enhance the mechanical performances of the composite in Young's modulus, fracture stress and strain. The dynamic kinetics of the vitrimer networks was controlled by the competition between accelerating effects of the added moieties of the grafted PCL shells, and the impeding effect of rigid CNC cores on the thermomechanical motion of surrounding polymer chains. Moreover, the CNC-PCL nanohybrids provided the enhanced interfacial compatibility from dispersed to cross-linked interactions with vitrimer networks, significantly improving the fracture resistance in stress and strain. Compared to the un-filled vitrimer, the nanohybrid vitrimer composite V15 exhibited the reinforced improvement in average Young's modulus of 2.5 ×, fracture stress of 5.4 × and fracture strain of 2.0 ×. We

believe that this research gains more insight into the synergistic interfacial compatibility between dynamic vitrimer networks and functional nanoparticles, paving the way for the design and application in advanced polymeric nanocomposites.

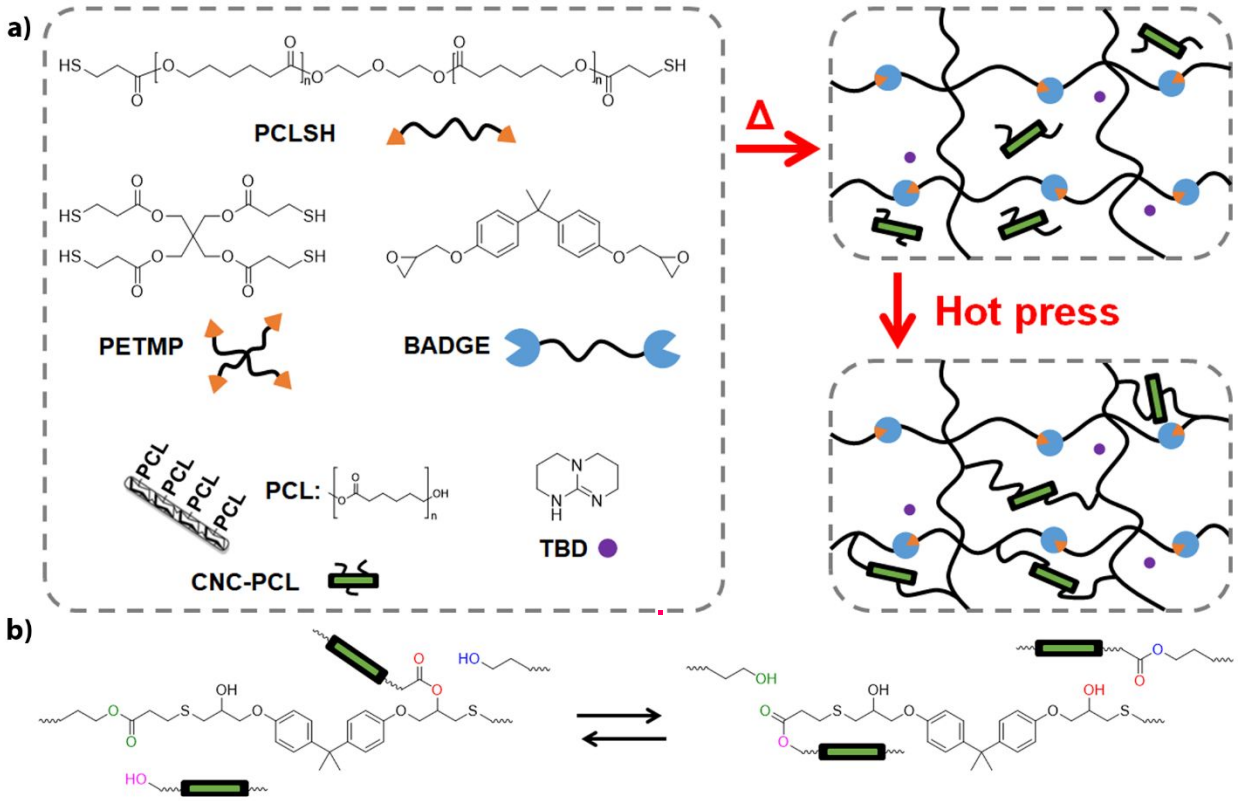

Figure 1. (a) Schematic illustration of epoxy-thiol vitrimers cross-linked with CNC-PCLs via epoxy-thiol 'click' reaction and hot-pressing transesterification process. (b) Carboxylate transesterification exchange reaction of epoxy-thiol vitrimers cross-linked with CNC-PCLs.

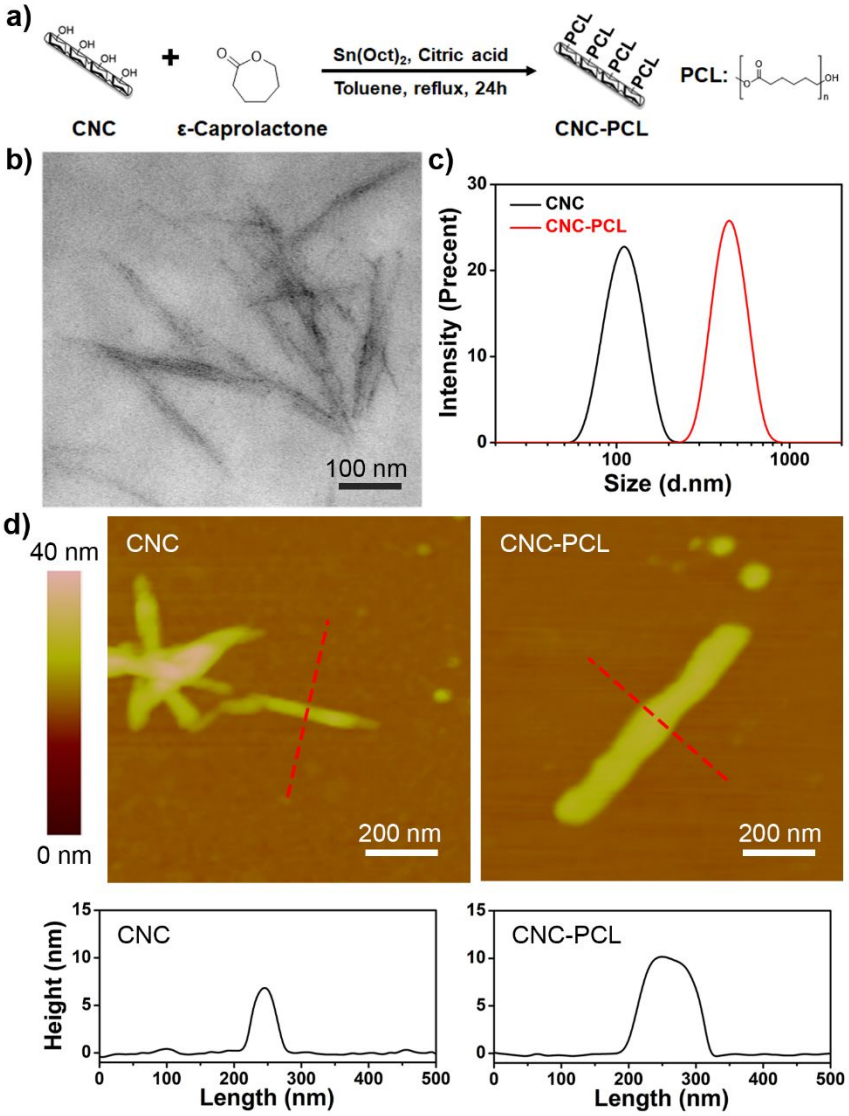

Figure 2. (a) Schematic illustration of PCL grafting from CNC surface. (b) TEM image of CNC-PCLs. (c) DLS analysis, (d) AFM topological images and surface profiles of CNCs and CNC-PCLs.

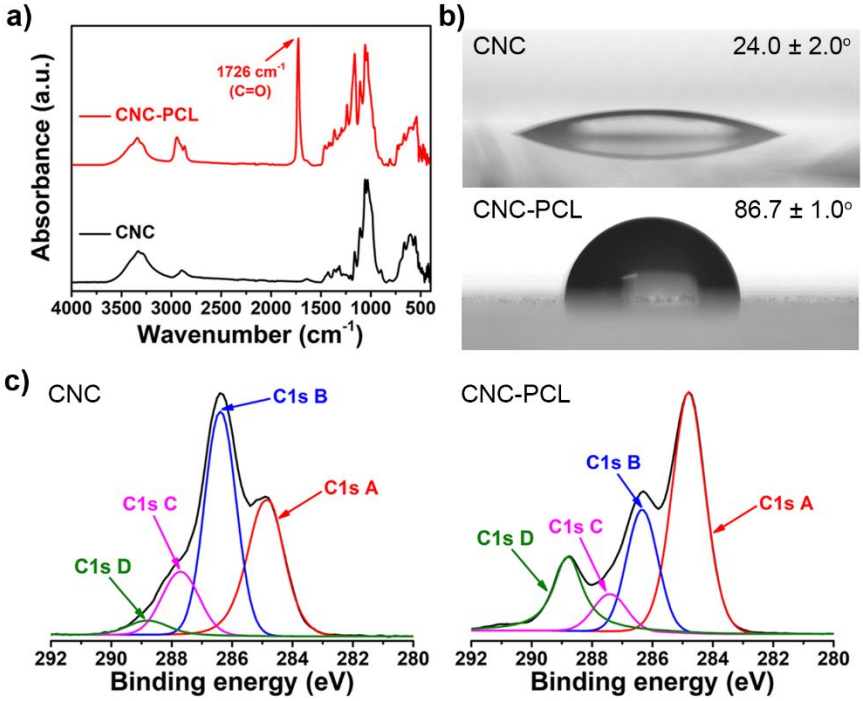

Figure 3. (a) ATR-FTIR spectra, (b) water contact angle and (c) high-resolution carbon peaks of XPS spectra of CNCs and CNC-PCLs.

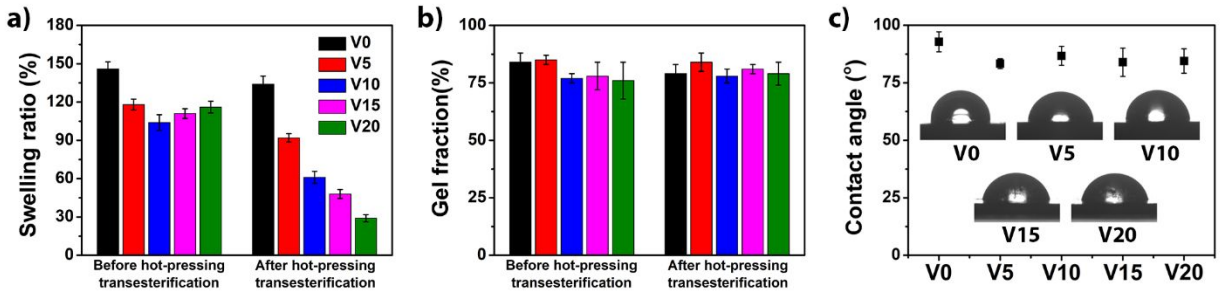

Figure 4. (a) Swelling ratio and (b) gel fraction of the vitrimers before and after cross-linking reaction via hot-pressing transesterification for 24 h. (c) The evolution of water contact angle of the vitrimers cross-linked with CNC-PCLs. Inset: Images of the water contact angle of vitrimers.

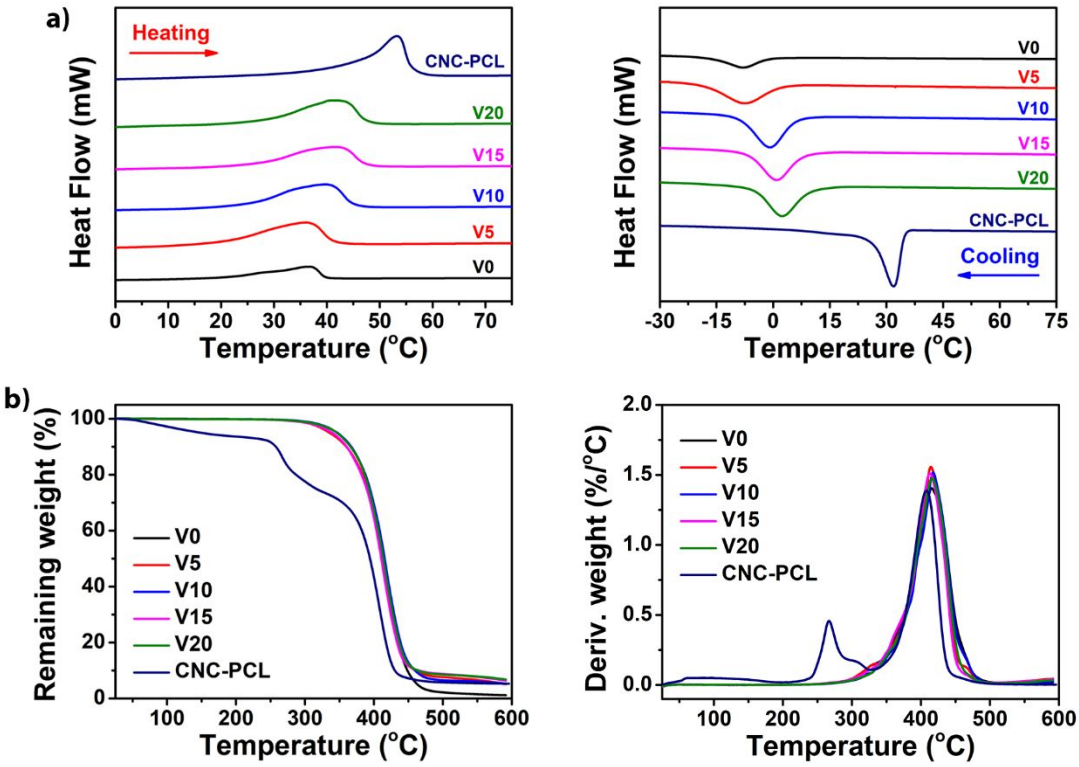

Figure 5. (a) DSC curves, (b) TGA curves of the nanohybrid vitrimer composites and CNC-PCL nanohybrids.

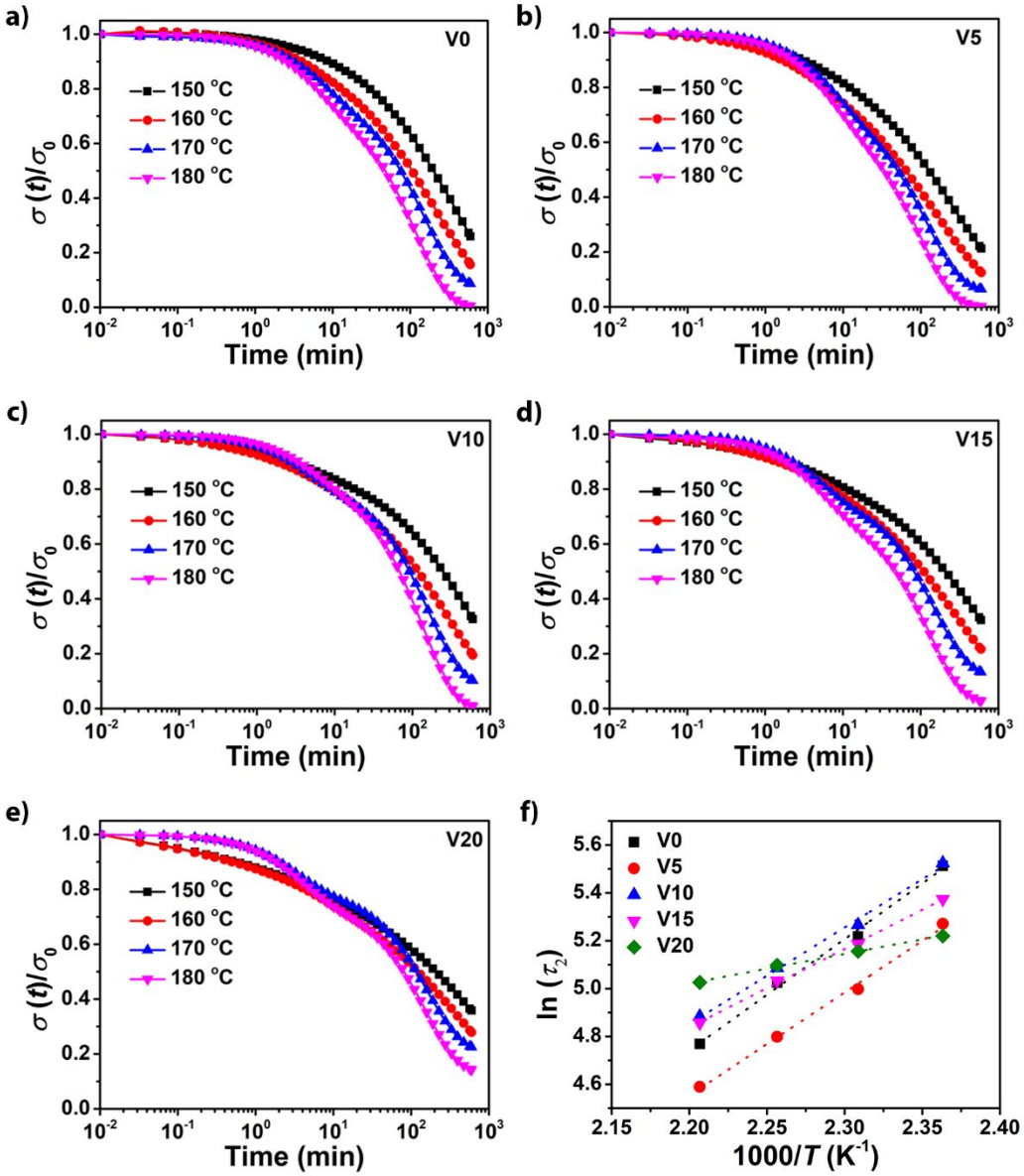

Figure 6. Normalized stress relaxation curves of (a) V0, (b) V5, (c) V10, (d) V15 and (e) V20. (f) Linear fitting of the $\ln(\tau_2)$ versus $1000/T$ of the vitrimer composites.

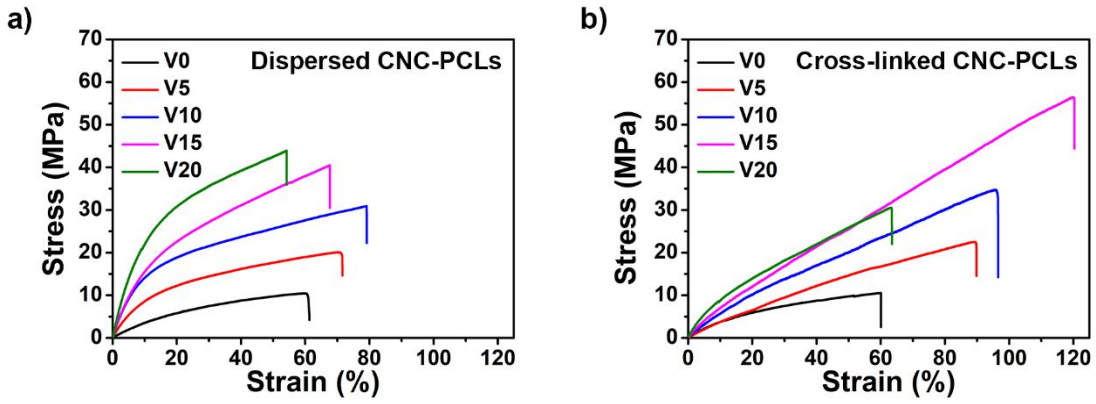

Figure 7. (a) Strain-stress curves of the vitrimer composites before and (b) after hot-pressing transesterification upon 1 MPa at 160 °C for 24 h.

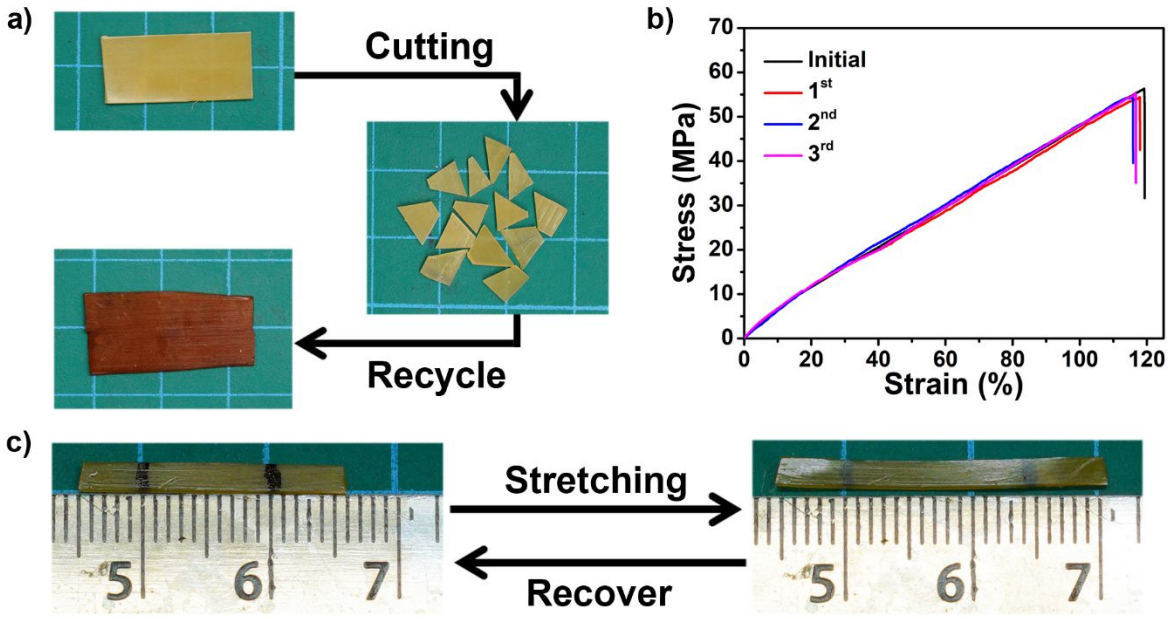

Figure 8. (a) Recycling of the nanohybrid vitrimer composites from cracked pieces to integrated bulk via hot-pressing reprocessing upon 1 MPa at 160 °C for 16 h. (b) Strain-stress curves of the

vitrimer composites V15 after recycling process. (c) The temporary shape via stretching deformation and the recovered shape memory effect via heating above 60 °C.

Table 1. Proportions of carbon atoms involved in various chemical bonds for CNC and CNC-PCL from XPS characterization

Sample	C1s A C-C/C-Hx (%)	C1s B C-OH (%)	C1s C O-C-O (%)	C1s D O-C=O (%)
CNC	34.62	46.21	15.34	3.83
CNC-PCL	50.62	23.65	7.67	18.06

Table 2. DSC data of the vitrimer composites and CNC-PCL nanohybrids

Sample	T_c (°C)	ΔH_c (J/g)	T_m (°C)	ΔH_m (J/g)	T_g (°C)
V0	-8.19	37.23	36.64	36.18	-42.31
V5	-7.60	31.89	36.09	34.83	-33.70
V10	-0.73	37.89	39.79	35.22	-27.22
V15	0.82	39.64	41.75	35.58	-19.68
V20	2.49	39.51	40.80	37.24	-11.96
CNC-PCL	31.95	45.63	53.20	46.17	-

Table 3. Activation energy of the transesterification exchange reaction of vitrimer composites

Sample	E_a (kJ/mol)	$\ln(\tau_0)$	$\Delta\tau_2$ at 150-180 °C (min)	Adjusted R^2
V0	38.67	-5.49	130.1	0.995
V5	35.84	-4.93	96.2	0.997
V10	33.54	-4.02	118.6	0.996
V15	27.20	-2.36	87.2	0.999
V20	10.20	2.32	32.6	0.997

ASSOCIATED CONTENT

Supporting Information.

The following files are available free of charge.

Synthesis and ^{1}H NMR spectra of PCLCl and PCLSH; TEM images, XPS spectra and TGA curve of the CNCs and CNC-PCLs; DSC curves, strain-stress curves and stress relaxation parameter and mechanical parameter of the vitrimer composites (PDF)

AUTHOR INFORMATION

Corresponding Author

*Boxin Zhao. E-mail: zhaob@uwaterloo.ca.

Author Contributions

The manuscript was written through contributions of all authors. All authors have given approval to the final version of the manuscript. ‡These authors contributed equally.

Notes

The authors declare no competing financial interest.

ACKNOWLEDGMENT

We are indebted to Prof. Tizazu H. Mekonnen's group for assistance with DMA measurement.

This work is supported by the Natural Sciences and Engineering Research Council of Canada (NSERC, grants RGPIN-2019-04650 and RGPAS-2019-00115).

REFERENCES

(1) Kloxin, C. J.; Scott, T. F.; Adzima, B. J.; Bowman, C. N. Covalent Adaptable Networks (Cans): A Unique Paradigm in Cross-Linked Polymers. *Macromolecules* 2010, *43*, 2643-2653.

(2) Bowman, C. N.; Kloxin, C. J. Covalent Adaptable Networks: Reversible Bond Structures Incorporated in Polymer Networks. *Angew. Chem., Int. Ed.* **2012**, *51*, 4272-4274.

(3) Kloxin, C. J.; Bowman, C. N. Covalent Adaptable Networks: Smart, Reconfigurable and Responsive Network Systems. *Chem. Soc. Rev.* **2013**, *42*, 7161-7173.

(4) Denissen, W.; Winne, J. M.; Du Prez, F. E. Vitrimers: Permanent Organic Networks with Glass-Like Fluidity. *Chem. Sci.* **2016**, *7*, 30-38.

(5) Montarnal, D.; Capelot, M.; Tournilhac, F.; Leibler, L. Silica-Like Malleable Materials from Permanent Organic Networks. *Science* **2011**, *334*, 965-968.

(6) Liu, T.; Zhao, B.; Zhang, J. Recent Development of Repairable, Malleable and Recyclable Thermosetting Polymers through Dynamic Transesterification. *Polymer* **2020**, *194*, 122392.

(7) Scheutz, G. M.; Lessard, J. J.; Sims, M. B.; Sumerlin, B. S. Adaptable Crosslinks in Polymeric Materials: Resolving the Intersection of Thermoplastics and Thermosets. *J. Am. Chem. Soc.* **2019**, *141*, 16181-16196.

(8) Guerre, M.; Taplan, C.; Winne, J. M.; Du Prez, F. E. Vitrimers: Directing Chemical Reactivity to Control Material Properties. *Chem. Sci.* **2020**, *11*, 4855-4870.

(9) Webber, M. J.; Tibbitt, M. W. Dynamic and Reconfigurable Materials from Reversible Network Interactions. *Nat. Rev. Mater.* **2022**, *7*, 541-556.

(10) Zheng, J.; Png, Z. M.; Ng, S. H.; Tham, G. X.; Ye, E.; Goh, S. S.; Loh, X. J.; Li, Z. Vitrimers: Current Research Trends and Their Emerging Applications. *Mater. Today* **2021**, *51*, 586-625.

(11) Sharma, H.; Rana, S.; Singh, P.; Hayashi, M.; Binder, W. H.; Rossegger, E.; Kumar, A.; Schlögl, S. Self-Healable Fiber-Reinforced Vitrimer Composites: Overview and Future Prospects. *Rsc Adv.* **2022**, *12*, 32569-32582.

(12) Wang, L.; Kelly, P. V.; Ozveren, N.; Zhang, X.; Korey, M.; Chen, C.; Li, K.; Bhandari, S.; Tekinalp, H.; Zhao, X.; Wang, J.; Seydibeyoğlu, M. Ö.; Alyamac-Seydibeyoglu, E.; Gramlich, W. M.; Tajvidi, M.; Webb, E.; Ozcan, S.; Gardner, D. J. Multifunctional Polymer Composite Coatings and Adhesives by Incorporating Cellulose Nanomaterials. *Matter* **2023**, *6*, 344-372.

(13) Heilmann, A. *Polymer Films with Embedded Metal Nanoparticles*; Springer: New York, 2003.

(14) Ramesh, G. V.; Porel, S.; Radhakrishnan, T. P. Polymer Thin Films Embedded with in Situ Grown Metal Nanoparticles. *Chem. Soc. Rev.* **2009**, *38*, 2646-2656.

(15) Pastoriza-Santos, I.; Kinnear, C.; Pérez-Juste, J.; Mulvaney, P.; Liz-Marzán, L. M. Plasmonic Polymer Nanocomposites. *Nat. Rev. Mater.* **2018**, *3*, 375-391.

(16) Liu, H.; Webster, T. J. Mechanical Properties of Dispersed Ceramic Nanoparticles in Polymer Composites for Orthopedic Applications. *Int. J. Nanomedicine* **2010**, *5*, 299-313.

(17) Kaur, S.; Gallei, M.; Ionescu, E. In *Organic-Inorganic Hybrid Nanomaterials*; Kalia, S., Haldorai, Y., Eds.; Springer: Cham, 2015, p 143-185.

(18) Jiang, Y.; Zhang, X.; Shen, Z.; Li, X.; Yan, J.; Li, B.-W.; Nan, C.-W. Ultrahigh Breakdown Strength and Improved Energy Density of Polymer Nanocomposites with Gradient Distribution of Ceramic Nanoparticles. *Adv. Funct. Mater.* **2020**, *30*, 1906112.

(19) Li, K.; Liu, B. Polymer-Encapsulated Organic Nanoparticles for Fluorescence and Photoacoustic Imaging. *Chem. Soc. Rev.* **2014**, *43*, 6570-6597.

(20) Jiang, Y.; Pu, K. Advanced Photoacoustic Imaging Applications of near-Infrared Absorbing Organic Nanoparticles. *Small* **2017**, *13*, 1700710.

(21) Sur, S.; Rathore, A.; Dave, V.; Reddy, K. R.; Chouhan, R. S.; Sadhu, V. Recent Developments in Functionalized Polymer Nanoparticles for Efficient Drug Delivery System. *Nano-Struct. Nano-Objects* **2019**, *20*, 100397.

(22) Dufresne, A. Cellulose Nanomaterial Reinforced Polymer Nanocomposites. *Curr. Opin. Colloid Interface Sci.* **2017**, *29*, 1-8.

(23) Wang, L.; Li, K.; Copenhaver, K.; Mackay, S.; Lamm, M. E.; Zhao, X.; Dixon, B.; Wang, J.; Han, Y.; Neivandt, D.; Johnson, D. A.; Walker, C. C.; Ozcan, S.; Gardner, D. J. Review on Nonconventional Fibrillation Methods of Producing Cellulose Nanofibrils and Their Applications. *Biomacromolecules* **2021**, *22*, 4037-4059.

(24) Ansari, F.; Berglund, L. A. Toward Semistructural Cellulose Nanocomposites: The Need for Scalable Processing and Interface Tailoring. *Biomacromolecules* **2018**, *19*, 2341-2350.

(25) Dufresne, A. Nanocellulose Processing Properties and Potential Applications. *Curr. For. Rep.* **2019**, *5*, 76-89.

(26) Wang, L.; Gardner, D. J.; Wang, J.; Yang, Y.; Tekinalp, H. L.; Tajvidi, M.; Li, K.; Zhao, X.; Neivandt, D. J.; Han, Y.; Ozcan, S.; Anderson, J. Towards Industrial-Scale Production of Cellulose Nanocomposites Using Melt Processing: A Critical Review on Structure-Processing-Property Relationships. *Composites: Part B* **2020**, *201*, 108297.

(27) Oksman, K.; Aitomäki, Y.; Mathew, A. P.; Siqueira, G.; Zhou, Q.; Butylina, S.; Tanpichai, S.; Zhou, X.; Hooshmand, S. Review of the Recent Developments in Cellulose Nanocomposite Processing. *Composites: Part A* **2016**, *83*, 2-18.

(28) Silva, F. A. G. S.; Dourado, F.; Gama, M.; Poças, F. Nanocellulose Bio-Based Composites for Food Packaging. *Nanomaterials* **2020**, *10*, 2041.

(29) Igarashi, Y.; Sato, A.; Okumura, H.; Nakatsubo, F.; Yano, H. Manufacturing Process Centered on Dry-Pulp Direct Kneading Method Opens a Door for Commercialization of Cellulose Nanofiber Reinforced Composites. *Chem. Eng. J.* **2018**, *354*, 563-568.

(30) Clemons, C.; Sabo, R. A Review of Wet Compounding of Cellulose Nanocomposites. *Polymers* **2021**, *13*, 911.

(31) Eichhorn, S. J.; Etale, A.; Wang, J.; Berglund, L. A.; Li, Y.; Cai, Y.; Chen, C.; Cranston, E. D.; Johns, M. A.; Fang, Z.; Li, G.; Hu, L.; Khandelwal, M.; Lee, K. Y.; Oksman, K.; Pinitsoontorn, S.; Quero, F.; Sebastian, A.; Titirici, M. M.; Xu, Z.; Vignolini, S.; Frka-Petesic, B. Current International Research into Cellulose as a Functional Nanomaterial for Advanced Applications. *J. Mater. Sci.* **2022**, *57*, 5697-5767.

(32) Djafari Petroudy, S. R.; Shojaeiarani, J.; Chabot, B. Recent Advances in Isolation, Characterization, and Potential Applications of Nanocellulose-Based Composites: A Comprehensive Review. *J. Nat. Fibers* **2023**, *20*, 2146830.

(33) Xu, C.; Zheng, Z.; Wu, W.; Fu, L.; Lin, B. Design of Healable Epoxy Composite Based on B-Hydroxyl Esters Crosslinked Networks by Using Carboxylated Cellulose Nanocrystals as Crosslinker. *Compos. Sci. Technol.* **2019**, *181*, 107677.

(34) Cudjoe, E.; Herbert, K. M.; Rowan, S. J. Strong, Rebondable, Dynamic Cross-Linked Cellulose Nanocrystal Polymer Nanocomposite Adhesives. *ACS Appl. Mater. Interfaces* **2018**, *10*, 30723-30731.

(35) Swartz, J. L.; Li, R. L.; Dichtel, W. R. Incorporating Functionalized Cellulose to Increase the Toughness of Covalent Adaptable Networks. *ACS Appl. Mater. Interfaces* **2020**, *12*, 44110-44116.

(36) Yue, L.; Amirkhosravi, M.; Ke, K.; Gray, T. G.; Manas-Zloczower, I. Cellulose Nanocrystals: Accelerator and Reinforcing Filler for Epoxy Vitrimerization. *ACS Appl. Mater. Interfaces* **2021**, *13*, 3419-3425.

(37) Yue, L.; Ke, K.; Amirkhosravi, M.; Gray, T. G.; Manas-Zloczower, I. Catalyst-Free Mechanochemical Recycling of Biobased Epoxy with Cellulose Nanocrystals. *ACS Appl. Bio Mater.* **2021**, *4*, 4176-4183.

(38) Habibi, Y.; Goffin, A.-L.; Schiltz, N.; Duquesne, E.; Dubois, P.; Dufresne, A. Bionanocomposites Based on Poly(ε-Caprolactone)-Grafted Cellulose Nanocrystals by Ring-Opening Polymerization. *J. Mater. Chem.* **2008**, *18*, 5002-5010.

(39) Labet, M.; Thielemans, W. Improving the Reproducibility of Chemical Reactions on the Surface of Cellulose Nanocrystals: Rop of ε-Caprolactone as a Case Study. *Cellulose* **2011**, *18*, 607-617.

(40) Casas, J.; Persson, P. V.; Iversen, T.; Córdova, A. Direct Organocatalytic Ring-Opening Polymerizations of Lactones. *Adv. Synth. Catal.* **2004**, *346*, 1087-1089.

(41) Okada, M. Chemical Syntheses of Biodegradable Polymers. *Prog. Polym. Sci.* **2002**, *27*, 87-133.

(42) Unger, M.; Vogel, C.; Siesler, H. W. Molecular Weight Dependence of the Thermal Degradation of Poly (ε-Caprolactone): A Thermogravimetric Differential Thermal Fourier Transform Infrared Spectroscopy Study. *Appl. Spectrosc.* **2010**, *64*, 805-809.

(43) Simão, J. A.; Bellani, C. F.; Branciforti, M. C. Thermal Properties and Crystallinity of Pcl/Pbsa/Cellulose Nanocrystals Grafted with Pcl Chains. *J. Appl. Polym. Sci.* **2017**, *134*, 44493.

(44) Bellani, C. F.; Pollet, E.; Hebraud, A.; Pereira, F. V.; Schlatter, G.; Avérous, L.; Bretas, R. E. S.; Branciforti, M. C. Morphological, Thermal, and Mechanical Properties of Poly(ε-Caprolactone)/Poly(ε-Caprolactone)-Grafted-Cellulose Nanocrystals Mats Produced by Electrospinning. *J. Appl. Polym. Sci.* **2016**, *133*, 43445.

(45) Meng, F.; Pritchard, R. H.; Terentjev, E. M. Stress Relaxation, Dynamics, and Plasticity of Transient Polymer Networks. *Macromolecules* **2016**, *49*, 2843-2852.

(46) Yang, Y.; Peng, G.; Wu, S.; Hao, W. A Repairable Anhydride-Epoxy System with High Mechanical Properties Inspired by Vitrimers. *Polymer* **2018**, *159*, 162-168.

(47) Capiel, G.; Hernández, E.; Marcovich, N. E.; Mosiewicki, M. A. Stress Relaxation Behavior of Weldable Crosslinked Polymers Based on Methacrylated Oleic and Lauric Acids. *Eur. Polym. J.* **2020**, *132*, 109740.

(48) Lian, W.; Han, H.; Zhang, X.; Peng, G.; Jia, Z.; Zhang, Z. Polyurethane Modified Epoxy Vitrimer and Its Stress Relaxation Behavior. *J. Polym. Eng.* **2021**, *41*, 365-374.

(49) Capelot, M.; Montarnal, D.; Tournilhac, F.; Leibler, L. Metal-Catalyzed Transesterification for Healing and Assembling of Thermosets. *J. Am. Chem. Soc.* **2012**, *134*, 7664-7667.

(50) Han, J.; Liu, T.; Hao, C.; Zhang, S.; Guo, B.; Zhang, J. A Catalyst-Free Epoxy Vitrimer System Based on Multifunctional Hyperbranched Polymer. *Macromolecules* **2018**, *51*, 6789-6799.

(51) Legrand, A.; Soulié-Ziakovic, C. Silica–Epoxy Vitrimer Nanocomposites. *Macromolecules* **2016**, *49*, 5893-5902.

(52) Huang, Z.; Wang, Y.; Zhu, J.; Yu, J.; Hu, Z. Surface Engineering of Nanosilica for Vitrimer Composites. *Compos. Sci. Technol.* **2018**, *154*, 18-27.

(53) Chen, X.; Li, L.; Wei, T.; Venerus, D. C.; Torkelson, J. M. Reprocessable Polyhydroxyurethane Network Composites: Effect of Filler Surface Functionality on Cross-Link Density Recovery and Stress Relaxation. *ACS Appl. Mater. Interfaces* **2019**, *11*, 2398-2407.

(54) Chen, M.; Si, H.; Zhang, H.; Zhou, L.; Wu, Y.; Song, L.; Kang, M.; Zhao, X.-L. The Crucial Role in Controlling the Dynamic Properties of Polyester-Based Epoxy Vitrimers: The Density of Exchangeable Ester Bonds (Y). *Macromolecules* **2021**, *54*, 10110-10117.

(55) Gao, M.; Wang, Y.; Li, S.; Liu, J.; Feng, A.; Zhang, G.; Zhang, L. Design and Fabrication of Recyclable and Reshape Vitrified Elastomer Reinforced with Renewable Cellulose Nanocrystal. *Compos. Commun* **2022**, *32*, 101165.

(56) Ran, Y.; Li, Y.-D.; Zeng, J.-B. Dynamic Crosslinking Towards Well-Dispersed Cellulose Nanofiber Reinforced Epoxy Vitrimer Composites. *Compos. Commun* **2022**, *33*, 101228.

(57) Shi, Y.; Hong, Y.; Hong, J.; Yu, A.; Lee, M. W.; Lee, J.; Goh, M. Bio-Based Boronic Ester Vitrimer for Realizing Sustainable and Highly Thermally Conducting Nanocomposites. *Composites: Part B* **2022**, *244*, 110181.

(58) Krishnakumar, B.; Sanka, R. V. S. P.; Binder, W. H.; Parthasarthy, V.; Rana, S.; Karak, N. Vitrimers: Associative Dynamic Covalent Adaptive Networks in Thermoset Polymers. *Chem. Eng. J.* **2020**, *385*, 123820.

(59) Hayashi, M. Implantation of Recyclability and Healability into Cross-Linked Commercial Polymers by Applying the Vitrimer Concept. *Polymers* **2020**, *12*, 1322.

(60) Alabiso, W.; Schlögl, S. The Impact of Vitrimers on the Industry of the Future: Chemistry, Properties and Sustainable Forward-Looking Applications. *Polymers* **2020**, *12*, 1660.

(61) Rodriguez, E. D.; Luo, X.; Mather, P. T. Linear/Network Poly(ε-Caprolactone) Blends Exhibiting Shape Memory Assisted Self-Healing (Smash). *ACS Appl. Mater. Interfaces* **2011**, *3*, 152-161.

(62) Zhao, Q.; Zou, W.; Luo, Y.; Xie, T. Shape Memory Polymer Network with Thermally Distinct Elasticity and Plasticity. *Sci. Adv.* **2016**, *2*, e1501297.

(63) Miao, W.; Zou, W.; Luo, Y.; Zheng, N.; Zhao, Q.; Xie, T. Structural Tuning of Polycaprolactone Based Thermadapt Shape Memory Polymer. *Polym. Chem.* **2020**, *11*, 1369-1374.

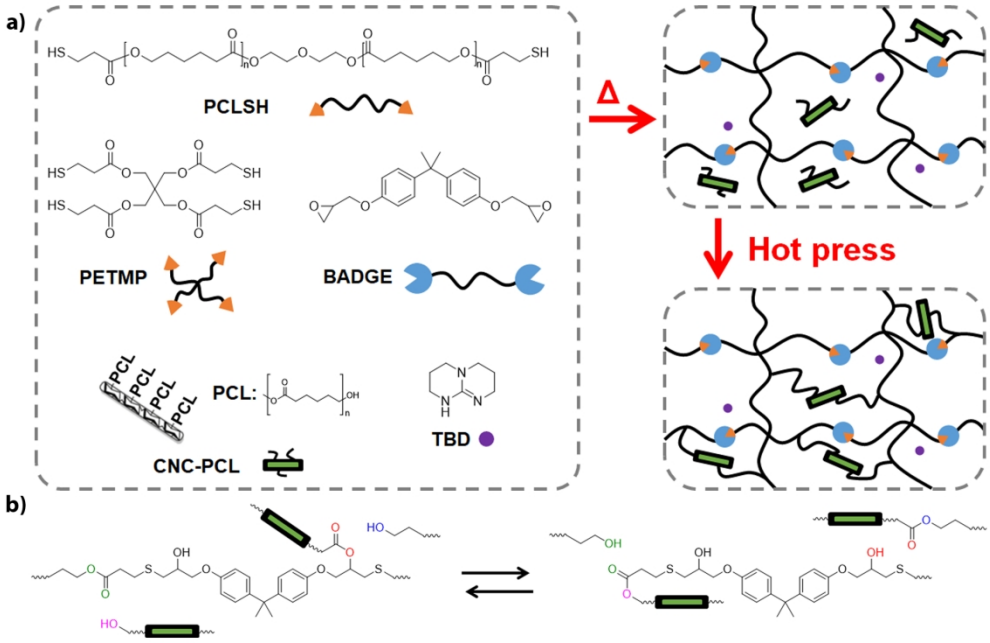

Figure 1. (a) Schematic illustration of epoxy-thiol vitrimers cross-linked with CNC-PCLs via epoxy-thiol 'click' reaction and hot-pressing transesterification process. (b) Carboxylate transesterification exchange reaction of epoxy-thiol vitrimers cross-linked with CNC-PCLs.

177x114mm (300 x 300 DPI)

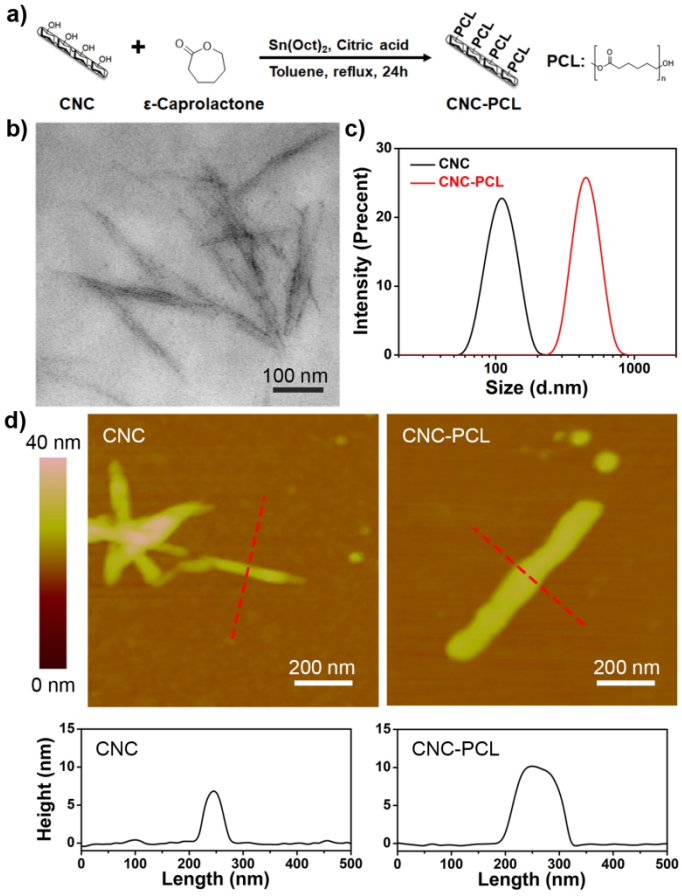

Figure 2. (a) Schematic illustration of PCL grafting from CNC surface. (b) TEM image of CNC-PCLs. (c) DLS analysis, (d) AFM topological images and surface profiles of CNCs and CNC-PCLs.

177x161mm (300 x 300 DPI)

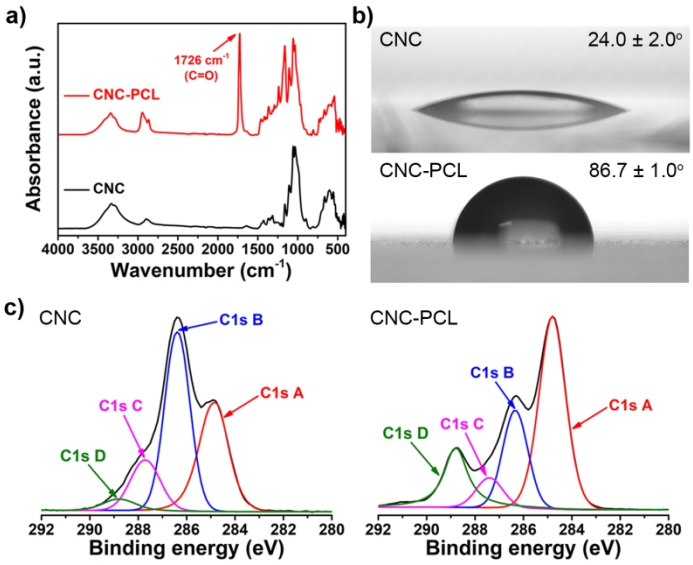

Figure 3. (a) ATR-FTIR spectra, (b) water contact angle and (c) high-resolution carbon peaks of XPS spectra of CNCs and CNC-PCLs.

177x100mm (300 x 300 DPI)

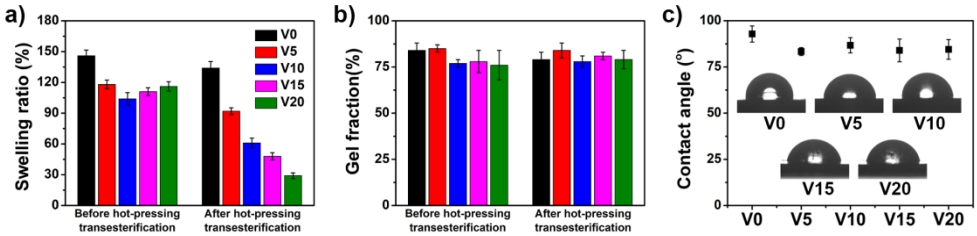

Figure 4. (a) Swelling ratio and (b) gel fraction of the vitrimers before and after cross-linking reaction via hot-pressing transesterification for 24 h. (c) The evolution of water contact angle of the vitrimers cross-linked with CNC-PCLs. Inset: Images of the water contact angle of vitrimers.

177x41mm (300 x 300 DPI)

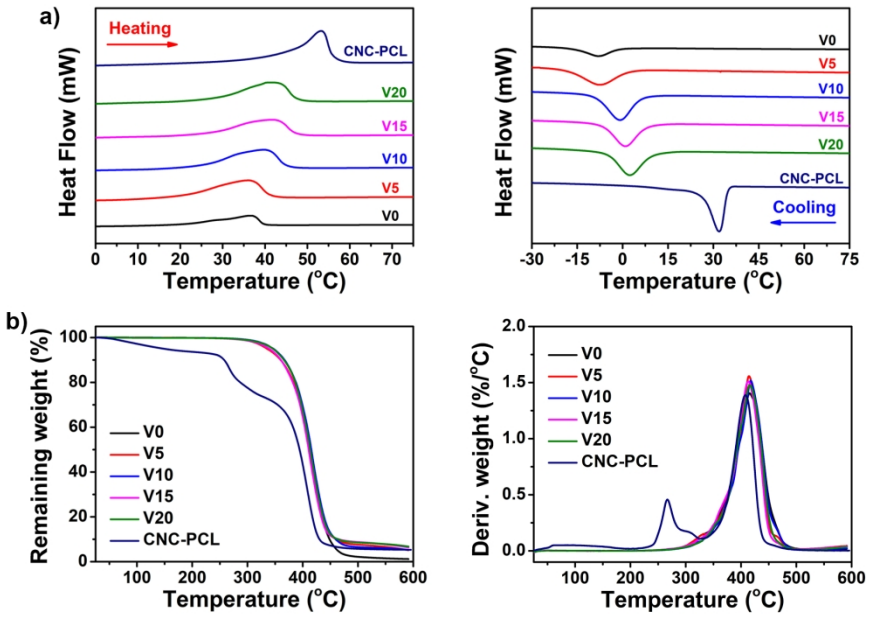

Figure 5. (a) DSC curves, (b) TGA curves of the nanohybrid vitrimer composites and CNC-PCL nanohybrids.

177x110mm (300 x 300 DPI)

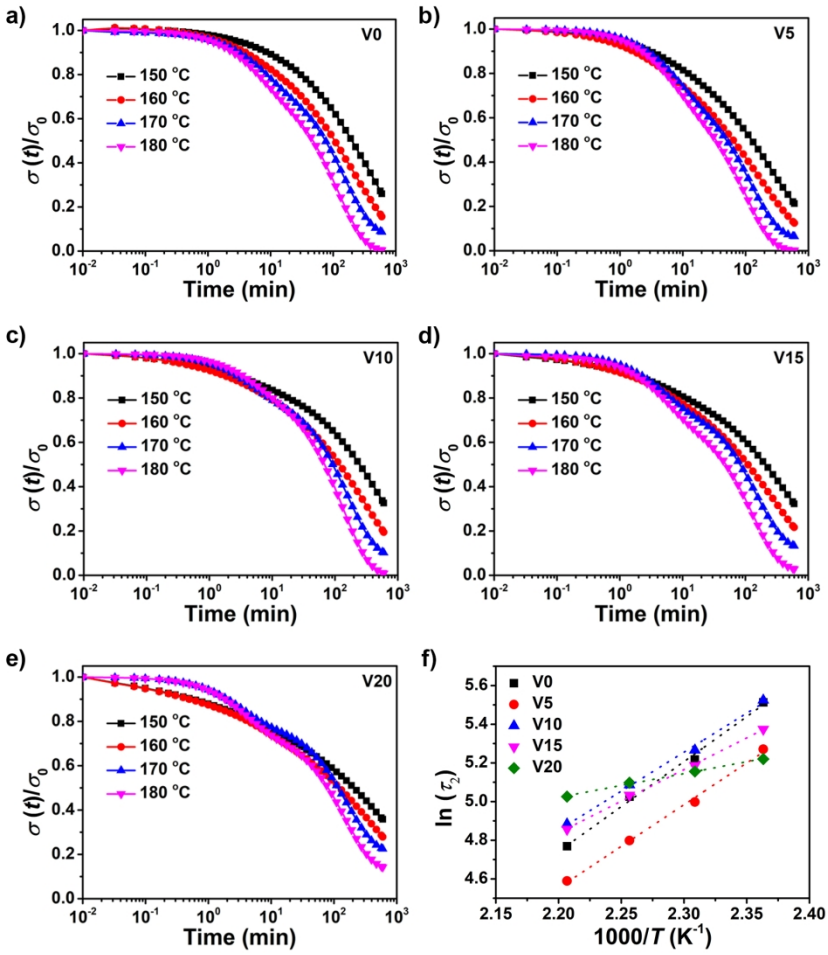

Figure 6. Normalized stress relaxation curves of (a) V0, (b) V5, (c) V10, (d) V15 and (e) V20. (f) Linear fitting of the ln(τ2) versus 1000/T of the vitrimer composites.

177x168mm (300 x 300 DPI)

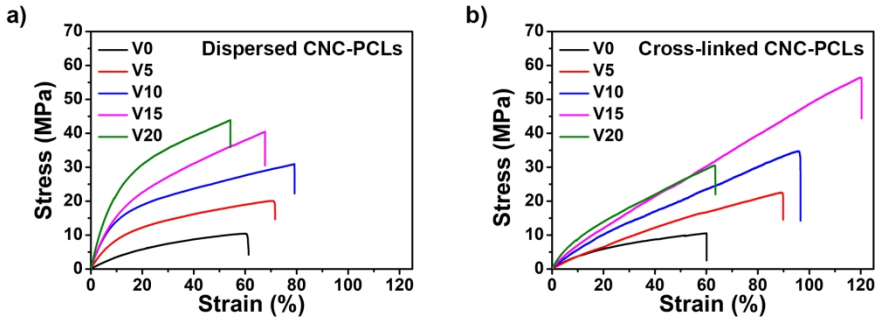

Figure 7. (a) Strain-stress curves of the vitrimer composites before and (b) after hot-pressing transesterification upon 1 MPa at 160 °C for 24 h.

177x58mm (300 x 300 DPI)

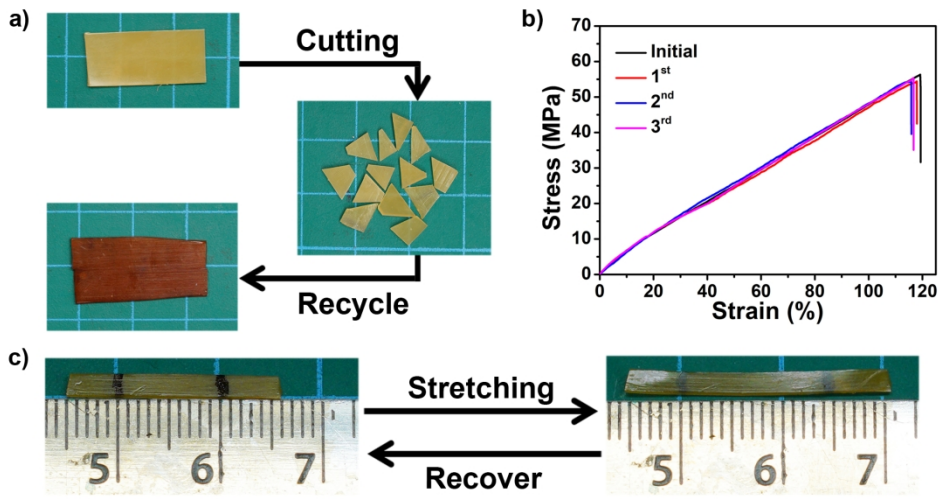

Figure 8. (a) Recycling of the nanohybrid vitrimer composites from cracked pieces to integrated bulk via hot-pressing reprocessing upon 1 MPa at 160 ☐C for 16 h. (b) Strain-stress curves of the vitrimer composites V15 after recycling process. (c) The temporary shape via stretching deformation and the recovered shape memory effect via heating above 60 ☐C.

177x90mm (300 x 300 DPI)